https://doi.org/10.5194/egusphere-2025-1373
Preprint. Discussion started: 9 April 2025

Summertime Arctic and North Atlantic-Eurasian Circulation Regimes under Climate Change

Johannes Max Müller[1], Oskar Andreas Landgren[2], and Dörthe Handorf[1]

[1]Alfred-Wegener Institute for Polar and Marine Research, Research Department Potsdam, Telegrafenberg A43, Potsdam, Germany
[2]Norwegian Meteorological Institute Institute, PO Box 43, Blindern, Oslo, Norway

Correspondence: Dörthe Handorf (doerthe.Handorf@awi.de)

Abstract. This study delves into the projected response of atmospheric circulation regimes, that are preferred and recurrent large-scale circulation patterns, to future climate change scenarios. We focus on the North Atlantic-Eurasian and Arctic regions in the boreal summer season. Using Simulated Annealing and Diversified Randomization (SAN) and K-means (KME) clustering methods, we analyse 20 global climate models from the CMIP6 ensemble to assess shifts in frequency of occurrence of circulation regimes for the end of the century under a high emission scenario. Additionally, storylines of summer Arctic climate change constrained by Barents–Kara Seas warming and Polar Amplification are incorporated to contextualize potential future atmospheric behaviours. Despite slight differences between the SAN and KME methods in identifying spatial regime structures, the fundamental spatial configuration of these regimes remains largely unchanged under future climate scenarios. Our analysis highlights the changing frequency of atmospheric circulation regimes under climate change. A significant occurrence change is detected for the North Atlantic Oscillation (NAO) regime by both methods, where positive phases are projected to become more frequent, consistent with previous studies. In the Arctic region, both clustering algorithms predict an increase in circulation regimes linked to negative pressure anomalies above the Arctic. This aligns with the projected increased occurrence of the positive NAO regime over the North Atlantic-Eurasian sector. Our analysis underscores that, while storylines provide a nuanced approach to exploring plausible climate futures, no consistent shifts in the occurrence of atmospheric circulation regimes emerge across the two studied storylines, possibly due to the small number of models representing each storyline. Furthermore, influences from regional climate changes such as Barents-Kara seas warming and Polar Amplification exhibit minimal impact on overarching circulation regimes. These findings contribute to an improved understanding of the sensitivity of atmospheric circulation regimes to climate change, with implications for predicting future extreme weather occurrences across these key regions.

1 Introduction

A long-standing concept for describing and understanding climate variability and change is the concept of atmospheric circulation regimes (see e.g. review by Hannachi et al., 2017). Regimes here refer to recurrent or quasi-stationary large-scale patterns of atmospheric circulation. Moreover, it is suggested that a weak external forcing acting on the dynamical system under consideration (in our case the atmosphere) does not change the spatial structure of the regime patterns, but instead leads to changes

https://doi.org/10.5194/egusphere-2025-1373
Preprint. Discussion started: 9 April 2025

in the frequency of occurrence of the regimes. On the other hand, a strong external forcing acting on the dynamical system can lead to significant changes in the spatial structure of the regime patterns or to the appearance of new regimes (Palmer, 1993; Corti et al., 1999). Based on these concepts, atmospheric circulation regimes have been a topic of research for the last 40 years in numerous studies.

Atmospheric circulation regimes provide the large-scale dynamical background and thereby are strongly related with regional weather conditions, including those which are favourable for development of extreme events like heat waves, cold spells or wind storms with potentially large impacts on the society (Cattiaux et al., 2010; Horton et al., 2015; Brunner et al., 2018; Schaller et al., 2018; Screen and Simmonds, 2010; Sousa et al., 2018).

The observed increase in extreme events (e.g. Coumou and Rahmstorf, 2012; Seneviratne et al., 2021) can be partly explained by global warming through thermodynamic arguments (Trenberth et al., 2015), and partly by changes in atmospheric circulation (Hoskins and Woollings, 2015), which are closely related to changes in atmospheric circulation regimes. For an enhanced understanding of recent and future extreme changes approaches which consider dynamical (e.g. changes in circulation regimes) and non-dynamical drivers have to be applied. For that purpose, storyline approaches have been developed (Trenberth et al., 2015; Shepherd, 2016; Shepherd et al., 2018).

A reliable detection of circulation changes in climate model simulations is often limited by a large uncertainty and low signal-to-noise ratios (Scaife and Smith, 2018; Smith et al., 2022). Therefore, it is needed to evaluate the ability of state-of-the art climate models to reproduce observed circulation regimes. On the other hand, there is a need to study future changes in atmospheric circulation regimes across multi-model ensembles of climate projections such as the Coupled Model Intercomparison Project (CMIP) to estimate uncertainty ranges for projected changes in regimes.

So far, most studies analysing the regime behaviour over the different CMIP generations have focused on the dynamically active boreal winter season (Babanov et al., 2023; Dorrington et al., 2022; Fabiano et al., 2021; Wiel et al., 2019). In a comprehensive study, Fabiano et al. (2021) analysed future changes in wintertime weather regimes over the Euro–Atlantic and Pacific–North American sectors based on CMIP5 and CMIP6 model ensembles. They evaluated the ability of the CMIP models to reproduce the spatial structure of the preferred regimes with an general improvement in the CMIP6 models. Furthermore, they analysed the future changes in the occurrence frequency and persistence of the regimes for different scenarios estimating e.g. significant positive trends in the frequency and persistence of NAO+ (North Atlantic Oscillation) in the future.

The boreal summer season was only considered in a few studies (Boé et al., 2009), as it is linked with lower variability of the atmospheric circulation in particular over the midlatitudes due to the decreased meridional temperature gradients and hence decreased baroclinic instability. Nonetheless, the boreal summer season is linked to many societal and ecological impacts at high-latitudes in the Northern Hemisphere. High-latitude fires, trans-Arctic shipping, and marine primary production are most pronounced during the warm season, and beside thermodynamical drivers, also changes in the atmospheric circulation may drive future changes in those impacts.

In order to develop mitigation strategies which rely on an awareness of the spread in climate change projections, storylines are introduced as suitable framework (Shepherd et al., 2018). They provide plausible realizations of climate change and emerge

https://doi.org/10.5194/egusphere-2025-1373
Preprint. Discussion started: 9 April 2025

from the range of climate projections found in a large ensemble of climate simulations. In the EU project POLARRES [1], four storylines have been identified (Levine et al., 2024) that represent different physical responses resulting from climate change in the Arctic region for the prolonged boreal summer season (May to October). Levine et al. (2024) analysed climate model simulations from the CMIP6 ensemble and grouped models according to these storylines of summer Arctic climate change constrained by Barents–Kara seas and Arctic tropospheric warming. Here, we analyse the full range of projected future atmospheric circulation changes in terms of circulation regime changes for the extended boreal summer season across an ensemble of CMIP6 models with the aim to answer the following questions:

1. What are the projected future changes in atmospheric circulation regimes under a strong future climate change scenario?
2. How sensitive are the results to different methodological aspects (classification method, spatial domain)?
3. How do the results differ for global models following different physically based storylines of summer Arctic climate change?

The paper is structured as follows: Section 2 presents the data, followed by the methods used to calculate circulation regimes. Statistical methods and the concept of storylines are introduced. The results and discussion are then presented in section 4, followed by a summary in section 5. An appendix completes the paper.

2 Data

In this study, the fifth generation ECMWF reanalysis (ERA5, Hersbach et al., 2020), is used as the reference dataset. Twenty state-of-the-art global climate models from the CMIP6 ensemble are included, listed in Section A. In examining the simulation of future time periods, the SSP5-8.5 emission scenario is of particular interest. As the highest emission scenario, it is characterised by a large increase in Greenhouse Gas (GHG) emissions, impinging a strong external forcing upon the atmosphere. Thus, a response of characteristics of circulation regimes is expected.

To analyse the characteristics of circulation regimes, the daily averaged sea level pressure (SLP) data are used. The North Atlantic-Eurasian region (30° N-90° N, 90° E-90° W) is considered, since the circulation regimes in this area are well-known. Since the main focus of the POLARRES project is however the Arctic region, we additionally analyse the circulation regimes over the circumpolar region from 50° N to 90° N. The extent of this region was varied and sensitivity of the results to this are discussed in section C. The extended boreal summer season from May to October is analysed, with a focus on two time periods, each spanning thirty years: the historical period from 1985-2014 and the future period from 2070-2099, as these two periods represent the last 30 years available from all models for the historical and future scenarios, respectively.

[1] https://polarres.eu/

https://doi.org/10.5194/egusphere-2025-1373
Preprint. Discussion started: 9 April 2025

3 Methods

3.1 Preprocessing

The following preprocessing procedure is adapted from Fabiano et al. (2021). First, the trend of the area-weighted season-averaged SLP time series of the respective area (North Atlantic-Eurasian: 30° N-90° N, Arctic: 50° N-90° N), is removed as background trend from the daily averaged SLP data for the historical and future model simulations and reanalysis data separately on their appropriate time period. Afterwards, SLP anomalies are obtained by substracting the mean seasonal cycle from the detrended data. Averaging the data day by day at each grid point yield the mean seasonal cycle. Additionally, a 21-day running mean is applied to remove higher-frequency fluctuations. The mean seasonal cycle calculated in the future time period may be affected by global warming as the mid-latitude circulation is influenced by GHG forcing (Woollings and Blackburn, 2012; Barnes and Polvani, 2013). This difference is taken into account by subtracting the historical seasonal cycle from both the historical and future time periods of climate model simulations as presented in Fabiano et al. (2021). Following the removal of the corresponding background trend and historical seasonal cycle, each dataset is interpolated onto the identical $1.125° \times 1.125°$ grid using bilinear interpolation.

3.2 Computation of Circulation Regimes

K-Means Clustering

In order to compute circulation regimes for the reanalysis ERA5 (blue pathway in Fig. 1), the SLP anomaly data undergo a process of dimensionality reduction through the implementation of an empirical orthogonal function (EOF) analysis (Lorenz, 1956). The first ten EOFs, which correspond to the eigenvectors of the covariance matrix of the original dataset, represent a substantial proportion of the dataset's variance and span the ten-dimensional reference state space. The explained variance cumulates to 66.3 % for the Atlantic-Eurasian region and 60.6 % for the Arctic region as stated in Fig. 1. The corresponding timeseries, the principal components (PCs) are defined as the scalar product between the data and eigenvectors. To obtain reference atmospheric circulation regimes, a K-Means clustering algorithm is applied in the ten-dimensional reduced state space. The PCs serve as the input data for the clustering algorithm. Each data point is assigned to its cluster centre, or centroid, which is selected to maximize inter-cluster distance while minimizing intra-cluster distance. In the case of the climate model data (red pathway in Fig. 1), the SLP anomalies are not reduced in their dimensionality via an EOF analysis. An alternative approach was taken, whereby the anomalies were projected onto the ten-dimensional reference state space. This results in the generation of pseudo-PCs. The pseudo-PCs afterward are clustered via the K-Means clustering algorithm to obtain simulated circulation regimes for each model simulation in both time periods that differ in their spatial structure compared to the reference circulation regimes.

In contrast, the projected approach (green pathway in Fig. 1) allocates the pseudo-PCs directly to the reference centroids, by finding their closest reference centroids (in terms of Euclidean distance) from the ERA5 reanalysis. This assignment of each day to the ERA5 reference clusters has been calculated for historical and future time periods.

https://doi.org/10.5194/egusphere-2025-1373
Preprint. Discussion started: 9 April 2025

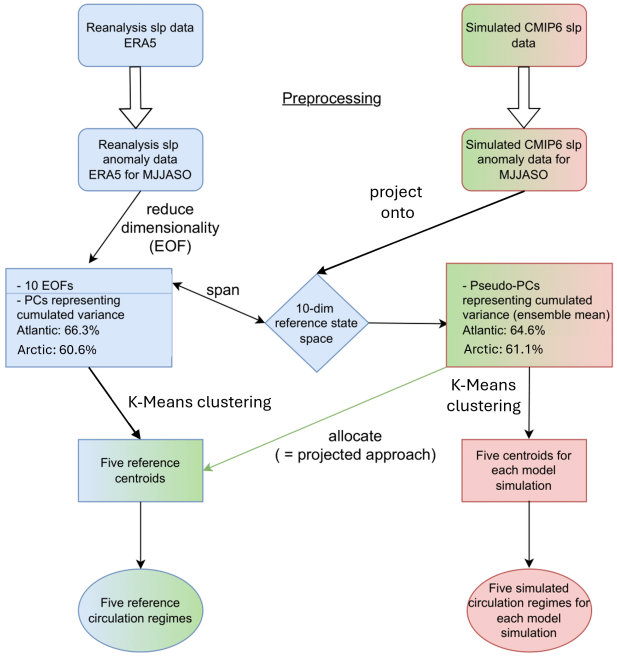

Figure 1. Chart flow of computation of atmospheric circulation regimes. The blue pathway indicates the approach to calculate reference circulation regimes. The red pathway shows the procedure to calculate simulated circulation regimes, the green pathway represents the projected regimes.

In order to provide a joint representation of the climate models' circulation regimes, the common simulated circulation regime framework is applied, which will be used to represent the characteristic joint regimes for the entire model ensemble. The common simulated circulation regime framework enables the possibility to compare the spatial structure between reanalysis and entire CMIP6 model ensemble. The dimensionality of the model data has been reduced through the application of a common EOF analysis, as detailed described in Benestad et al. (2023). The input data for the common EOF is obtained by merging the preprocessed data of each climate model into a single data file along the temporal axis. The common EOFs span a 10-dimensional common state space, similar to the reference approach. The explained variance for the Atlantic-Eurasian region is again higher, cumulating to 64.6 %, while 61.1 % of the variance for the Arctic region is explained by the common EOFs. Common PCs serve as input data for the K-Means clustering algorithm that is applied. Five common simulated circulation regimes are obtained for each time period, representing the joint regimes for the entire model ensemble.

SANDRA

In order to investigate the sensitivity of the results to the choice of clustering method, a second method was also applied. Simulated annealing and diversified randomisation clustering (SANDRA, Philipp et al., 2007) differs from K-means clustering by introducing a randomised cluster assignment inspired by the thermally induced movement of atoms in a crystal lattice (hence the term "annealing", from the process in metallurgy). A cooldown factor is used to gradually decrease the movements, resulting in a positioning which is numerically very efficient at finding solutions close to the global optimum. Details are found in Philipp et al. (2007). The application in the present study is based on the implementation in the cost733class software (Philipp et al., 2016). Comparisons of SANDRA with other methods show very favourable results (Røste and Landgren, 2022; Tveito and Huth, 2016).

In contrast to the K-Means clustering algorithm, we only followed the projected approach for SANDRA, i.e. the SANDRA algorithm was trained on the ERA5 reanalysis data and then the resulting five regimes were assigned to all climate models, for both the historical and future periods. The SANDRA method was applied for both the $1.125°$ horizontal resolution used in KME method as well as a coarser $2.5°$ resolution. Unsurprisingly, the resulting regimes were almost identical (with spatial

https://doi.org/10.5194/egusphere-2025-1373
Preprint. Discussion started: 9 April 2025

correlation > 0.998 for all 5 patterns, and maximum absolute difference below 0.5 hPa, not shown), and we decided to use the coarser resolution for computational efficiency.

Determining the Number of Clusters

In almost all clustering algorithms, the number of clusters must be predetermined, and this is a topic of extensive discussion in the literature, as referenced in the following sources: Stephenson et al. (2004); Madonna et al. (2017); Straus et al. (2007); Crasemann et al. (2017). Here, an elbow test (Olmo et al., 2024, see Appendix B) was conducted to ascertain whether it was feasible to identify an optimal number of centroids. According to this test and supported by the silhouette score (Rousseeuw, 1987, see Appendix B) the number of clusters is set to five for both regions. This is in agreement with cluster numbers in other studies, e.g. in Crasemann et al. (2017) a Monte-Carlo simulation was performed to determine the number of clusters in the winter season for the North Atlantic-Eurasian region, resulting in 5 clusters.

Further Methods

The performance of models in reproducing the spatial structure of reference circulation regimes is evaluated using a Taylor diagram (Taylor, 2001). This method incorporates three statistical measures: the spatial correlation coefficient (R) between simulated and reference regimes, the normalized standard deviation (SD) of anomalies, and the root-mean-square error (RMSE). These metrics are plotted on a polar diagram, where the angular axis represents R, the radial axis indicates SD, and the distance from the reference point reflects the RMSE. The Taylor diagram provides a compact visualization of model performance, aiding in the comparison of spatial structures.

To determine statistical significance of the changes in frequency of occurrence under the influence of rising GHG emission in the future for both regions, Welch's t-test is employed (Welch, 1947). Welch's t-test is a robust tool for comparing group means, and is particularly effective when variances are unequal. Here we use it to evaluate whether observed differences in the frequency of circulation regimes are statistically significant compared to historical records, providing insights into potential climate-related anomalies in future projections.

3.3 Storylines

In the context of climate research, the term "storyline" is used to group together climate models that exhibit a certain physically consistent response in their future climate change. This approach emphasizes an understanding of the driving factors behind climate events and their plausibility, without the assignment of a priori probabilities. The use of multiple storylines allows for the exploration of a range of potential futures. This approach raises risk awareness by framing risks in an event-oriented manner, which aligns with how people perceive risk. Additionally, it strengthens decision-making by integrating climate change information with other factors to address compound risks. As argued in Levine et al. (2024), a considerable proportion of the variability in the surface climate response to global warming in the Arctic during the extended summer season is linked to the warming of the Barents-Kara Sea (BK) and the Arctic lower troposphere (Polar Amplification, PA). We therefore concentrate

https://doi.org/10.5194/egusphere-2025-1373
Preprint. Discussion started: 9 April 2025

on the two storylines determined by the opposite signals in these two factors. Following the results from Levine et al. (2024), these storylines can be most closely represented by the four CMIP6 models presented in Table 1.

Strong Barents-Kara-Sea Warming (BK+) Weak Polar Amplification (PA−)	Weak Barents-Kara-Sea Warming (BK−) Strong Polar Amplification (PA+)
CNRM-CM6-1 CNRM-ESM2-1	KACE-1-0-G NorESM2-MM

Table 1. Storyline and respective model selection

4 Results & Discussion

4.1 North Atlantic-Eurasian Region

Five atmospheric circulation regimes are detected in the North Atlantic-Eurasian region. The reference circulation regimes from ERA5 obtained with the K-Means clustering (KME) and the SANDRA (SAN) algorithm are summarised below. Overall, very similar SLP anomaly patterns were also found in Riebold (2023) who investigated the same region for the summer season from June to August.

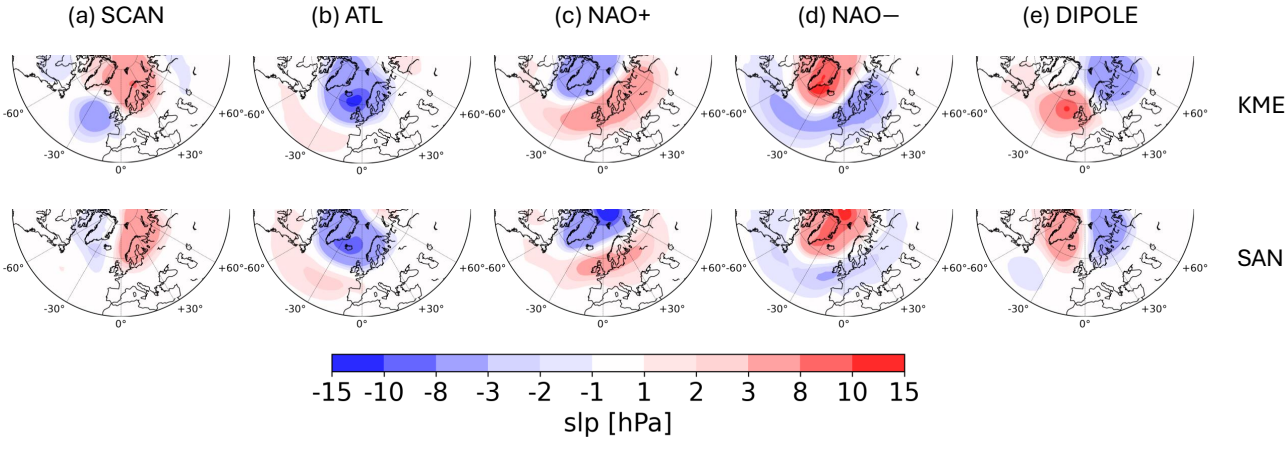

Figure 2. Reference circulation regimes for the North Atlantic-Eurasian region in the extended summer season, May to October, in the historical time period (1985-2014) from the ERA5 dataset, calculated by the K-Means (KME) and SANDRA (SAN) algorithms.

– The Scandinavian Ural Blocking (SCAN), shown in Fig. 2a, indicates a positive pressure anomaly centered above Scandinavia and a low pressure anomaly, which extends from the British Isles to the North Atlantic Ocean (referring to KME, Fig. 2a upper row) and is centered above Greenland regarding the pattern determined by the SAN algorithm. Both centers

https://doi.org/10.5194/egusphere-2025-1373
Preprint. Discussion started: 9 April 2025

of action are also found in the Atlantic low regimes determined in analyses of summer (June-August) circulation regimes over the North Atlantic (20°-80°N, 90°W-30°E) by Boé et al. (2009) and Cattiaux et al. (2013).

- The Atlantic Trough (ATL) is characterized by a strong negative pressure anomaly centered above the British Isles, depicted in Fig. 2b.
- Fig. 2c displays the North Atlantic Oscillation in its positive phase (NAO +). Here an elongated positive pressure anomaly extends from the Ural to Newfoundland contrasted by a negative pressure anomaly above Greenland. The pattern calculated by the SAN algorithm is spatially more confined compared to that of the KME method. Similar patterns have been detected by (Boé et al., 2009, NAO +), and (Cattiaux et al., 2013, Atlantic Ridge).
- Fig. 2d displays the North Atlantic Oscillation in negative phase (NAO −), here the positive and negative pressure anomalies are swapped respective to NAO +.
- The Dipole Atlantic Blocking regime (DIPOLE) describes a positive pressure anomaly centered between Iceland and Ireland in the patterns from KME, and appears shifted northward towards Greenland in the patterns calculated by the SAN method. The positive pressure anomaly is opposing the negative pressure anomaly that is located at the Barents Sea. The regime is shown in Fig. 2e and also found in Boé et al. (2009) as Atlantic ridge pattern.

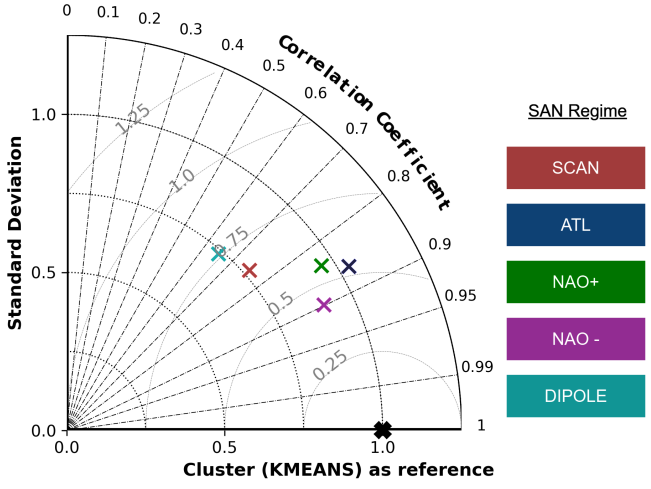

Figure 3. Taylor diagram analysis of circulation regimes computed by KME and SAN algorithms in the historical period for the North Atlantic-Eurasian region in extended boreal summer season from May to October. The reference circulation regimes computed from ERA5 reanalysis data with KME is marked as black cross, the colored crosses represent the SAN regimes.

The agreement between the characteristic regime patterns of both algorithms, KME and SAN, is evaluated by means of a Taylor plot in Fig. 3, where the KME patterns serve as reference. The correlation coefficient for all clusters are above 0.65 and the spatial standard deviation of the patterns obtained with the SAN method are close to the reference values. Three patterns, i.e. ATL, NAO + and NAO − exhibit very high spatial correlation values above 0.8. The spatial similarity between the clusters calculated from KME and SAN algorithm is validated by these findings. For the SCAN and DIPOLE patterns, the correlation coefficient is between 0.65 and 0.8. The standard deviation value yields values around 0.75 for SCAN (0.65 for DIPOLE). The negative pressure anomaly facing the positive pressure anomaly above Scandinavia in the SCAN pattern from SAN algorithm, refer Fig. 2a, is decreased in its magnitude compared to the pattern computed from KME, resulting in the low standard deviation value. Additionally,

https://doi.org/10.5194/egusphere-2025-1373
Preprint. Discussion started: 9 April 2025

the center of the negative pressure anomaly of the SAN pattern is shifted northwards compared to the KME pattern, corresponding to a spatial correlation coefficient of 0.75. Vice versa, the same arguments of shifting and decreasing magnitudes in the characteristic pressure anomalies can be made for the DIPOLE pattern in Fig. 2e) resulting in a spatial correlation coefficient of 0.65. To summarise, both algorithms KME and SAN detected very similar summer circulation regimes.

In section 3.2 two different methods to calculate circulation regimes within the KME framework for the simulation models were presented: the projected approach and the simulation circulation regime approach. The simulated common circulation regimes for the extended boreal summer season, revealing the joint regimes for the whole ensemble of climate models for the future period, exhibit small differences in their spatial structure compared to the reference circulation regimes computed from reanalysis ERA5 data. The evaluation by means of a Taylor plot is presented in Fig. 4 for the North Atlantic-Eurasian region. The calculated common simulated circulation regimes in the future period exhibit high spatial correlation coefficients with the reference circulation regimes from the ERA5 reanalysis data in the historical period. The correlation coefficients reach values above 0.85 for all five regimes and the standard deviations of the common simulated circulation regimes are found to be in close proximity to the reference values.

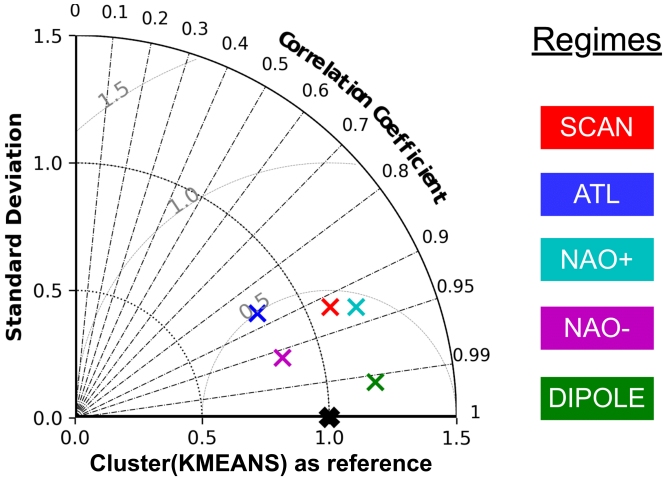

Figure 4. Taylor Diagram of the simulated circulation regimes derived from the common EOFs of CMIP6 models in the future time period under GHG forcing, corresponding to the SSP5-8.5 scenario in the extended boreal summer season from May to October. These regimes are compared to those calculated from ERA5 reanalysis data, which serves as a reference point.

These results support the hypothesis put forth in Section 1, namely that a weak external forcing acting on the dynamical system—in this case, the external forcing on the atmosphere—does not alter the spatial structure of the regime patterns. Thus, the spatial structure of the summer circulation regimes does not change significantly under the influence of rising GHG emission in the future time period compared to the historical time period. This allows us to apply the projected approach for the calculation of the frequency of regime occurrence for the climate models in the historical and future period. Additionally, the projected approach is able to calculate the frequency of occurrence of the circulation regimes of the CMIP6 models more accurately than the simulated circulation regime approach. This is visualised in Fig. 5. For both regions, the absolute difference between the simulated respective projected and reference circulation regimes frequencies averaged over all regimes for each model in the historical period, i.e. the frequency bias as defined in Fabiano et al. (2021) is shown. The mean frequency bias is smaller for the projected circulation regimes compared to the simulated circulation regimes. The interquartile range of the projected circulation regimes' frequency bias is lower compared to the interquartile range of the simulated circulation regimes' frequency bias. Fabiano et al. (2021) suggested that a lower frequency bias results in a higher confidence to project changes in the frequency of occurrence under climate change.

https://doi.org/10.5194/egusphere-2025-1373
Preprint. Discussion started: 9 April 2025

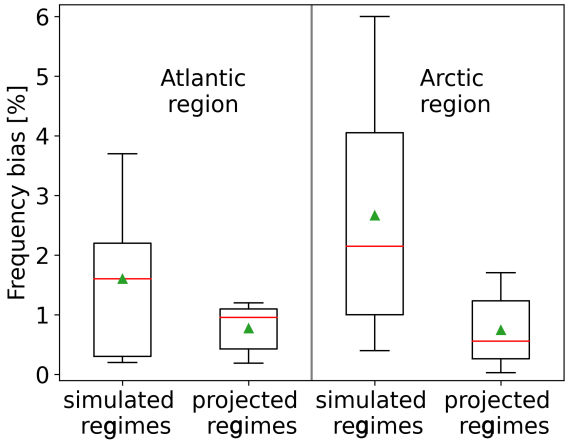

Figure 5. Box plot of frequency biases for North Atlantic-Eurasian and Arctic region of simulated (respective projected) circulation regimes compared to the reference circulation regimes in the historical period. The median is shown as a red line, the mean is indicated as a green triangle. The boxes represent the first and third quartiles, the top and bottom bars denote the 10^{th} and 90^{th} percentiles.

Due to this, the projected approach is preferable in the analysis of changes in the frequency of occurrence for both regions.

We now turn to analyse the projected future changes under the SSP5-8.5 scenario. The changes in the frequency of occurrence for circulation regimes computed by both methods, KME and SAN, are shown in Fig. 6. The change in the frequency of occurrence for a pattern is the difference between the percentage of days assigned to that particular pattern in the future (2070-2099) and in the historical time period (1985-2014) in the extended boreal summer season from May to October. This is calculated for each of the twenty CMIP6 models, with the spread of the models visualised in the box plot.

For both methods, i.e. SAN and KME, the NAO + pattern occurs significantly more frequent in the future period compared to the historical period under the GHG forcing projected by the SSP5-8.5 scenario. The models representing the storyline linked with a strong Barents-Kara-Sea warming (BK +) and weak Polar Amplification (PA −) are simulated to occur even more often in the future time period compared with the other storyline (BK−/PA+). The NAO − pattern is projected to decrease in their frequency of occurrence significantly in the future, as detected with both algorithms. In Boé et al. (2009), who analysed a more confined region in the summer season utilising CMIP3 climate models, an increase in NAO + and decrease in NAO − was also found, supporting the presented findings. Regarding the SCAN pattern, both methods detected a decrease in the frequency of occurrence in the future for most of the models but the change is not statistically significant for the SAN algorithm. Regarding the ATL and DIPOLE patterns both methods show diverging future changes, which again are not significant for the SAN method.

To summarise, both methods, the KME and SAN calculate typical circulation regimes for the North Atlantic-Eurasian region, which are similar in their spatial structure, only exhibiting small differences at the location of the centers of characteristic SLP anomalies. The simulated changes in the spatial structure due to the influence of climate change in the atmosphere are small for the whole ensemble of climate models, but the frequency in occurrence is altered as suggested by Corti et al. (1999), see also the Introduction section 1. Both methods simulate a significant increase in the occurrence of the NAO + pattern in the future under strong GHG forcing, the SAN method's simulated change is higher in its median and interquartile range. The same applies for the projected the NAO − regime, both methods simulate a significant decrease in their frequency of occurrence. Only for the NAO + pattern there is a tendency of models associated with BK+/PA− storyline to occur even more often.

https://doi.org/10.5194/egusphere-2025-1373
Preprint. Discussion started: 9 April 2025

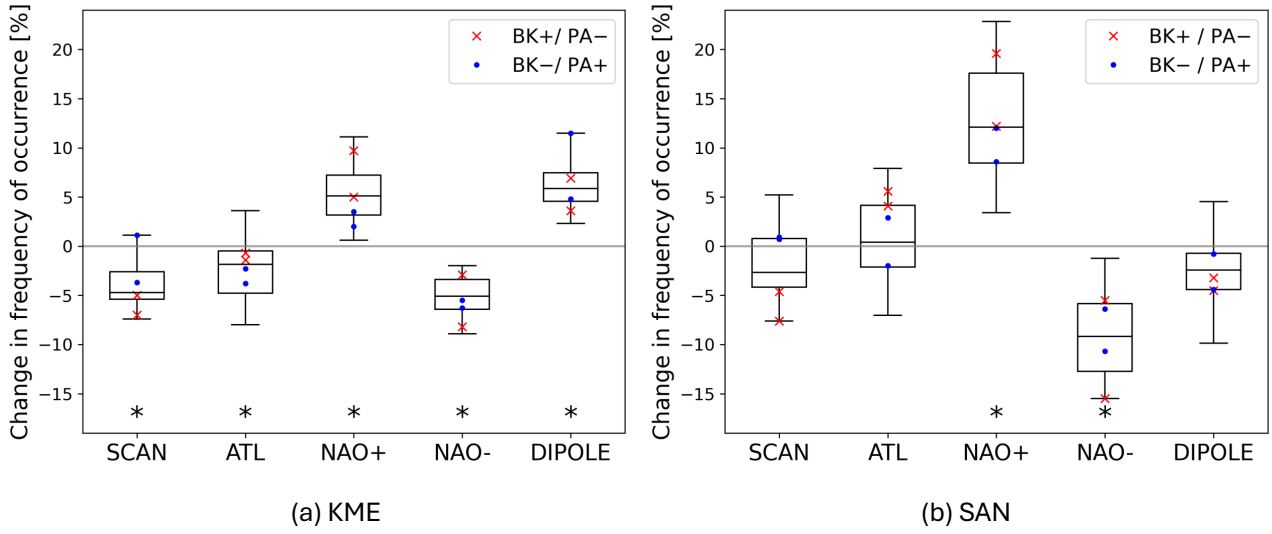

Figure 6. Changes in the frequency of occurrence for the North Atlantic-Eurasian region under global warming (SSP5-8.5 scenario) compared to the historical period, in the extended boreal summer season May to October. The boxes denote the first and third quartiles, the center black line indicates the ensemble median and the top and bottom whiskers represent the 10^{th} and 90^{th} percentiles. Stars indicate significant changes compared to the historical data at the 95% confidence level calculated with Welch's t-test.

4.2 Arctic Region

For the Arctic region, five atmospheric circulation regimes are determined based on the arguments in 3.2. The reference patterns calculated by both methods, KME and SAN, for the ERA5 data are shown in Fig. 7.

- Greenland-Siberia Dipole1(Fig. 7a) is characterized by a negative pressure anomaly above Iceland and Greenland facing a positive pressure anomaly above Siberia resulting in a strong westerly flow across the Arctic region.
- Bering-Svalbard Dipole (Fig. 7b) is characterized by a positive pressure anomaly centered above Greenland and extending towards the Barents Sea and a negative pressure anomaly centered at Kamchatka.
- Arctic Ocean High (AO +, Fig. 7c) is a (strong) positive pressure anomaly above the Arctic Ocean.
- Arctic Ocean Low (AO −, Fig. 7d) displays a (strong) negative pressure anomaly is centered above the Arctic. Note that AO + and AO − have very similar patterns but with opposite sign.
- East-West Dipole (Fig. 7e) shows a negative pressure anomaly above the Barents Sea which extends to the Laptev Sea when using the KME method. A positive pressure anomaly is also found in the pattern calculated by the SAN algorithm

https://doi.org/10.5194/egusphere-2025-1373
Preprint. Discussion started: 9 April 2025

opposing the negative pressure anomaly. For the KME method, the positive pressure anomaly is above the North Atlantic Sea.

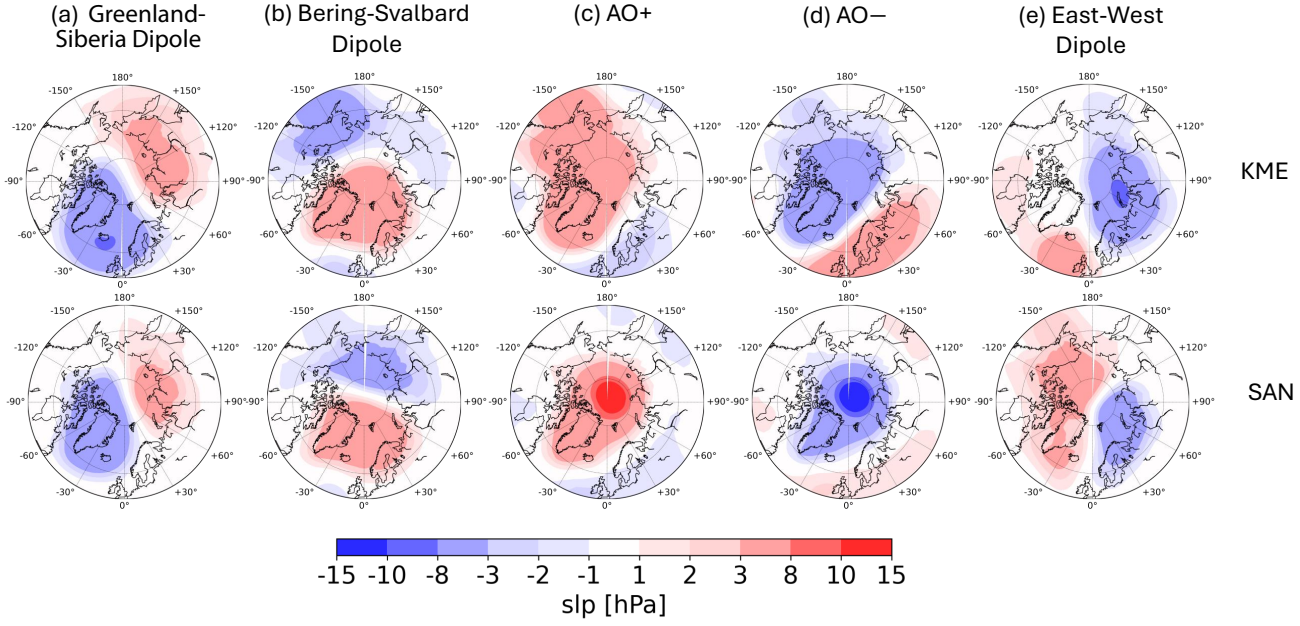

Figure 7. Reference circulation regimes for the Arctic region in the historical time period (1985-2014) from the ERA5 reanalysis dataset, calculated by the K-Means Clustering (KME) and simulated annealing and diversified randomisation clustering (SAN) algorithms.

Similar to the North Atlantic-Eurasian region, the spatial patterns obtained by both methods are compared by a Taylor plot in Fig. 8, where the patterns calculated by the KME algorithm serve as reference. The regimes show correlation coefficients between 0.7 and 0.9, thus the spatial structure of every pattern is similar for both methods, KME and SAN. The standard deviations of the magnitudes of the SLP anomalies are close to the reference for Bering-Svalbard Dipole, AO − and East-West Dipole. Greenland-Siberia Dipole exhibits a standard deviation below 0.7, that is also visible in Fig. 7a, since the pressure anomalies are smaller. Regarding AO + in Fig. 7c, the SAN pattern shows a stronger positive pressure anomaly above the Arctic, that is represented by a high standard deviation in the Taylor plot above 1.5. To conclude, both methods, KME and SAN, calculate clusters with similar spatial structure for the Arctic region in the extended boreal summer season May to October in the historical time period 1985-2014 from ERA5 reanalysis data.

Based on the arguments in section 4.1 and the findings of the box plot in Fig.5, the projected approach is used to analyse the changes in the regime occurrence frequencies between the historical and future period for the Arctic region. These results are shown in Fig. 9 for both methods, KME and SAN. For the regimes calculated by the KME algorithm, KME Bering-Svalbard Dipole and KME AO +, occur less frequently in the future which is in agreement with the results obtained

https://doi.org/10.5194/egusphere-2025-1373
Preprint. Discussion started: 9 April 2025

by the SAN algorithm. The occurrence of Greenland-Siberia Dipole is not changing significantly in its frequency of occurrence in the future period in the ensemble median for both methods. KME AO − and KME East-West Dipole patterns occur significantly more often in the future time period. In contrast, the SAN East-West Dipole pattern exhibits a negative change in the frequency of occurrence under GHG forcing in the future. This may be due to the shifted positive pressure anomaly in the SAN algorithm compared to the KME algorithm. An increase in the frequency of occurrence is simulated in the future time period compared to the historical time period for SAN AO − in accordance with the predicted changes from the KME method. Similar to the North Atlantic-Eurasian region, the interquartile range of the frequency changes for the SAN regimes is greater compared to the KME regimes.

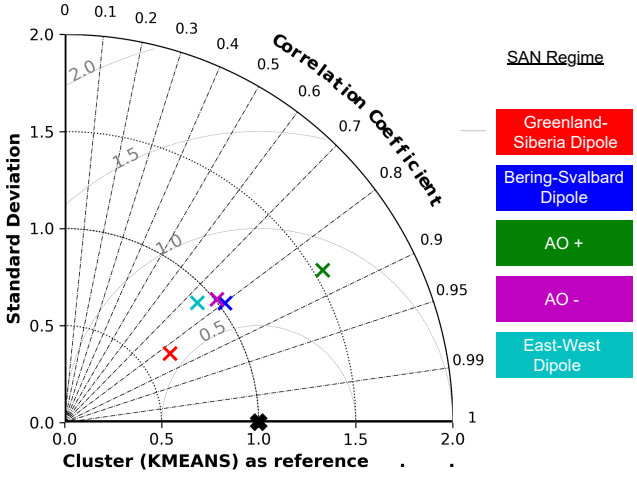

Figure 8. Taylor diagram analysis of circulation regimes computed by KME and SAN algorithms in the historical period for the Arctic region in extended boreal summer season from May to October. The reference circulation regimes computed from ERA5 reanalysis data with KME is marked as black cross. The colored crosses represent the respective regime calculated from SAN algorithm.

Considering the spatial patterns shown in Fig. 7, the circulation regime characterized by a negative pressure anomaly above the Arctic center; AO − is simulated to occur more frequently in the future period for both investigated algorithms. This change is consistent with the increase in the frequency of occurrence of the NAO + regime found in the North Atlantic-Eurasian region in the future time period, since both patterns, AO − and NAO + exhibit spatial similarities, i.e. a negative pressure pressure anomaly above Greenland and a broad positive pressure anomaly above Northern Europe (see Figs. 2c and 7d). The circulation regimes associated with positive pressure anomalies above the Arctic; Bering-Svalbard Dipole and AO + are expected to occur less frequently in the future. Again, AO + and NAO − (from the analysis over the North Atlantic-Eurasian region) are both characterized by a positive pressure anomaly above Greenland and a negative pressure anomaly extending from the Ural to the North Atlantic. Regarding the SAN algorithm, the circulation regime East-West Dipole is characterized by a slight positive pressure anomaly above the Arctic. Consistent with SAN DIPOLE findings in the North-Atlantic region, this cluster is projected to occur less frequently in the future. In contrast, the KME algorithm predicts that East-West Dipole and KME DIPOLE will become more frequent under global warming. This difference might be due to the positive pressure anomaly in the KME DIPOLE and KME East-West Dipole pattern (Fig. 7e), which is shifted southwards compared to the SAN patterns.

Considering especially the frequency changes for those models which represent the two storylines BK +/PA − and BK −/PA +, we detected a consistent change only for the AO − pattern. Both methods reveal a stronger increase in the change in frequency of occurrence for the BK +/PA − storyline. This is in accordance with the results for the NAO + regime (section 4.1, Fig. 6). The finding is supported by Fig. 10, that shows the storylines of summer Arctic climate change for SLP. Fig. 10b shows the

https://doi.org/10.5194/egusphere-2025-1373
Preprint. Discussion started: 9 April 2025

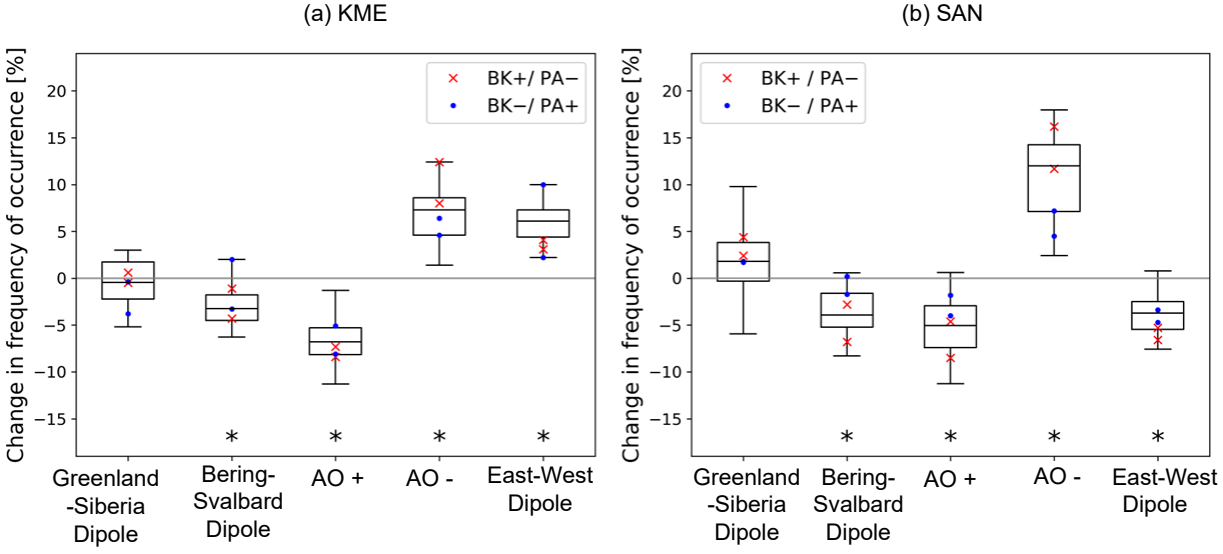

Figure 9. Changes in the frequency of occurrence for the North Atlantic-Eurasian region under global warming compared to the historical period, SSP5-8.5 scenario in the extended summer season May to October. The boxes denote the first and third quartiles, the center black line indicated the ensemble median and the top and bottom whiskers represent the 10^{th} and 90^{th} percentiles. The star indicated a significant changes compared to the historical data at the 95% confidence level calculated with Welch's t-test.

change in SLP in the Multi-Model-Mean per degree warming indicating a decrease in SLP above the Arctic under global warming in the extended boreal summer season from May to October. The decrease in SLP above the Arctic is weakened (note different scales) for models representing the storyline BK−/ PA+ in Fig. 10c and is amplified for the models associated with the BK+/ PA− storyline, refer Fig. 10a. The decrease in the SLP above the Arctic under global warming underscores the simulated change in the frequency of occurrence for AO − and NAO + since these patterns are characterized by an Arctic negative pressure anomaly and positive pressure anomaly above Northern Europe.

To summarize, the calculated circulation regimes of both methods, KME and SAN, are similar in their spatial structure when analysing the Arctic region in the extended boreal summer season from May to October. The simulated changes in the frequency of occurrence utilising the projection approach show a significant increase for the regime AO − for both methods. The patterns Bering-Svalbard Dipole and AO + are projected to decrease significantly in their frequency of occurrence under the influence of a strong GHG scenario in the future for both methods. The interquartile ranges obtained with the SAN approach are generally higher than those obtained with the KME approach.

https://doi.org/10.5194/egusphere-2025-1373
Preprint. Discussion started: 9 April 2025

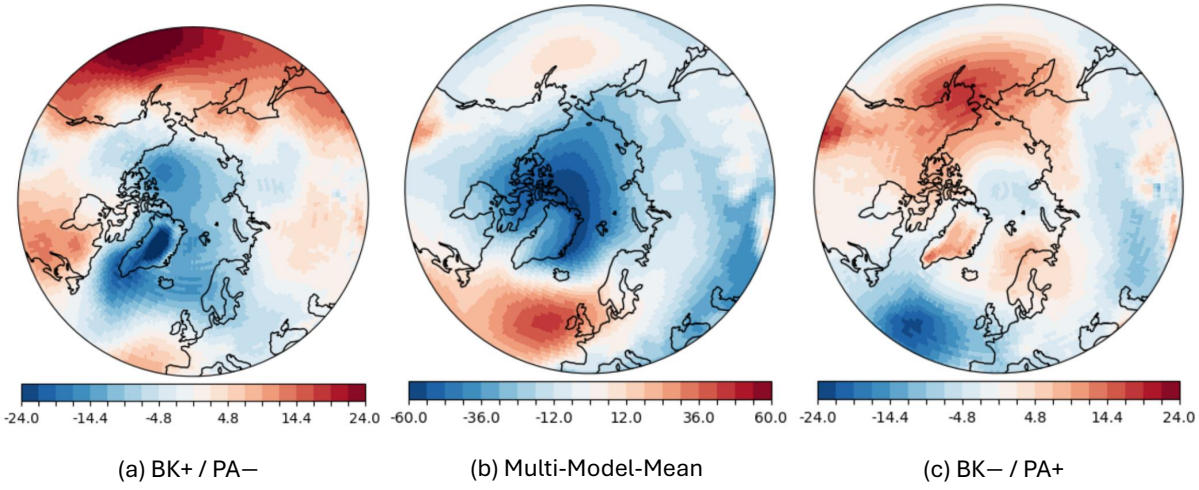

Figure 10. Storylines and Multi-Model-Mean of climate change for SLP (units: hPa/K). Note that the scale for the colorbar for the multimodel mean in b) differs from the scale used for the storylines in a) and c).

5 Conclusions and Outlook

This study investigates the impact of climate change on atmospheric circulation regimes in the North Atlantic-Eurasian and Arctic regions, focusing on their spatial structure, frequency of occurrence, and the respective changes along two specific storylines of summer Arctic climate change. Clustering algorithms (SAN and KME) and statistical analyses were used to assess the robustness of regime changes under the projected climate scenario SSP5-8.5.

The spatial structure analysis revealed consistent patterns between SAN and KME algorithms, identifying similar but not identical circulation regimes. Notably, no significant changes in spatial patterns were observed under future climate scenarios, suggesting resilience in the spatial organization of atmospheric circulation.

The frequency of occurrence analysis has highlighted agreement between the two methods, with the results obtained by the SAN method showing a slightly stronger response and larger spread across the ensemble of CMIP6 models to future projections. In the North Atlantic-Eurasian region, the consistent increase in the positive North Atlantic Oscillation (NAO+) regime aligns with existing literature. For the Arctic, where regime analyses are sparse, both algorithms projected consistent changes, offering valuable insights into how the Arctic atmospheric circulation responds to climate change. These findings emphasize the importance of regional assessments to capture the unique responses of distinct geographical areas to global climate change.

The storyline analysis revealed limited influence of localized drivers, such as Barents-Kara warming and Polar Amplification, on large-scale circulation regimes. This highlights the complexity of regional processes and the need for continued research into the interplay between local climatic factors and broader atmospheric patterns.

https://doi.org/10.5194/egusphere-2025-1373
Preprint. Discussion started: 9 April 2025

The leading questions proposed in the introduction may be answered as follows:

1. What are the projected future changes in atmospheric circulation regimes under a strong future climate change scenario?

Under the SSP5-8.5 scenario, significant changes are projected in the frequency of atmospheric circulation regimes. The frequency of the positive North Atlantic Oscillation (NAO +) is expected to increase, consistent with prior research. This applies also to the simulated frequency changes of the AO − Arctic pattern which has similar pressure anomaly characteristics compared to NAO +. In contrast, the opposing circulation regime, i.e. NAO − is consistently simulated to occur less often in both methods. For the Arctic region, patterns associated with a negative pressure anomaly above the Arctic center (AO −) are expected to increase in their occurrence. Patterns linked with a positive pressure anomaly (AO +, Bering-Svalbard Dipole) are simulated to decrease in their frequency of occurrence. The spatial structure of these regimes remains largely unchanged, supporting the concept of Corti et al. (1999), that suggests stability of spatial regime structure under a weak external forcing on a dynamical system.

2. How sensitive are the results to different methodological aspects (classification method, spatial domain)?

The study employs two distinct clustering methods: K-Means (KME) and simulated annealing and diversified randomisation (SAN). Both methods identify similar spatial structures of circulation regimes, with minor variations in cluster details. Results remain robust across different spatial domains. This sensitivity analysis underlines the methodological consistency in identifying circulation patterns.

3. How do the results differ for global models following different physically based storylines?

The study integrates storylines of summer Arctic climate change constrained by Barents-Kara Sea warming and Polar Amplification to evaluate variations in projected outcomes. Models linked to strong Barents-Kara Seas warming (BK+) and weak Polar Amplification (PA−) show a tendency for increased occurrence of NAO + and the AO − Arctic pattern that are linked to negative pressure anomalies above the Arctic and positive pressure anomalies above Northern Europe. In contrast, models associated with weak BK warming (BK−) and strong PA (PA+) exhibit a reduced magnitude of the changes in the frequency of occurrence for NAO + and AO −. For the other patterns, no significant differences were detected for models associated with either of the storylines. It can be hypothesised that two models linked to each storyline are insufficient to find robust results. Depending on their availability, it would be worthwhile to analyse a greater sample size of models to potentially identify additional representative models for each storyline, including multiple realisations of each model.

Finally, there are a few details we did not delve deeper into. The coupled nature of the CMIP models allows more in-depth analysis of how changes in other parts of the climate system (e.g. sea-surface temperature or snow cover) affect the detected changes in the atmospheric circulation regimes and vice versa. We did not analyse the mechanisms behind the circulation

https://doi.org/10.5194/egusphere-2025-1373
Preprint. Discussion started: 9 April 2025

changes as this would require other types of analysis frameworks (for instance causal network theory). From the literature, it is clear that the number of circulation patterns to use is often debated, as the number depends on many different considerations. We have chosen to focus on the relatively low number five, both because it corresponds with well-known regimes from the literature, especially for the North Atlantic, but also because of our performed analyses on two metrics, the Distortion score and the Silhouette score in Appendix B. Nevertheless, the presented results provide some insight in future changes of atmospheric circulation regimes in the previously not so well-studied boreal summer season.

Code availability. The code is available under https://github.com/ravenclaw00/WCD_ACR_paper

Appendix A: List of Considered CMIP6 Climate Models

Table A1 lists the CMIP6 models that were examined in this study, along with their constituent ensemble members and relevant references.

Appendix B: Number of Considered Circulation Regimes

The following scores are specific to the KME algorithm. The Elbow plot (Olmo et al., 2024) illustrates the distortion score, which describes the within-cluster sum of squared distances and is often employed to assess the efficiency of the formation and allocation of centroids, namely the efficiency of the K-Means clustering algorithm. In Fig. B1, the Distortion score is generated

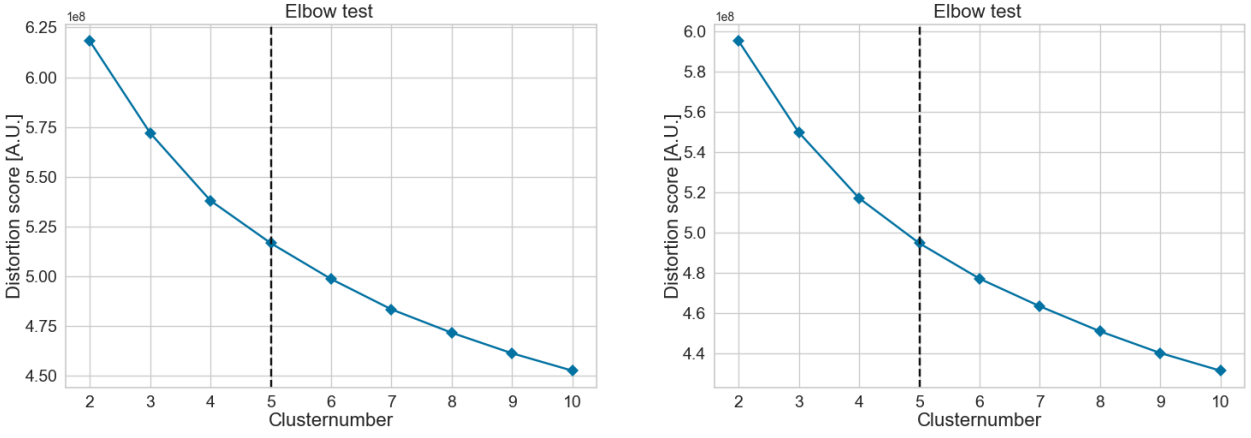

(a) North Atlantic-Eurasian region (b) Arctic region

Figure B1. Distortion score of the dataset considered for the respective region. The row specifies the investigated region, the column shows the results for different numbers of clusters

https://doi.org/10.5194/egusphere-2025-1373
Preprint. Discussion started: 9 April 2025

Model	Member	Reference
ACCESS-CM2	r1i1p1f1	Bi et al. (2020)
ACCESS-ESM1-5	r1i1p1f1	Ziehn et al. (2020)
CESM2-WACCM	r1i1p1f1	Danabasoglu et al. (2020)
CNRM-CM6-1	r1i1p1f2	Voldoire et al. (2019)
CNRM-CM6-1-HR	r1i1p1f2	Voldoire et al. (2019)
CNRM-ESM2-1	r1i1p1f2	Seferian (2018)
GFDL-CM4	r1i1f1p1	Held et al. (2019)
GFDL-ESM4	r1i1p1f1	Dunne et al. (2020)
HadGEM3-GC31-LL	r1i1p1f3	Williams et al. (2018)
INM-CM4-8	r1i1p1f1	Volodin et al. (2019)
INM-CM5-0	r1i1p1f1	N/A
IPSL-CM6A-LR	r1i1p1f1	Boucher et al. (2020)
KACE-1-0-G	r1i1p1f1	Byun et al. (2019)
MIROC6	r1i1p1f1	Tatebe et al. (2019)
MIROC-E3SL	r1i1p1f2	Hajima et al. (2020)
MPI-ESM1-2-HR	r1i1p1f1	Mauritsen et al. (2019)
MPI-ESM1-2-LR	r1i1p1f1	Mauritsen et al. (2019)
MRI-ESM2-0	r1i1p1f1	Yukimoto et al. (2019)
NorESM2-MM	r1i1p1f1	Seland et al. (2020)
UKESM1-0-LL	r1i1p1f2	Sellar et al. (2019)

Table A1. Examined CMIP6 models, their ensemble member, and the references.

using the KElbow Visualizer package from Python. The algorithm calculates the elbow point, which is defined as the point of greatest curvature in the curve. The KElbow Visualizer suggests that five clusters represent an optimal number of clusters for both regions, the North Atlantic-Eurasian and Arctic, for the extended boreal summer season from May to October.

To substantiate the chosen number, the silhouette coefficient value is evaluated and illustrated in Fig. B2 for both regions. The silhouette score is a metric utilised to assess the quality of clustering, whereby the cohesion and separation of clusters are measured. The average distance between data points within the same cluster is defined as cohesion, whereas the average distance between data points in one cluster and the nearest neighboring cluster is defined as separation. The silhouette coefficient value ranges from -1 to 1 and was developed by Rousseeuw (1987). A positive silhouette score indicates the presence of well-defined and separated clusters. Conversely, a negative score suggests the existence of overlapping or poorly defined clusters. The mean silhouette score for both regions is approximately 0.08, although the coefficient for the North Atlantic-Eurasian region is greater than the Arctic region's one. For each cluster number index, the silhouette coefficient value is positive, validating the choice of the cluster number for both regions.

https://doi.org/10.5194/egusphere-2025-1373
Preprint. Discussion started: 9 April 2025

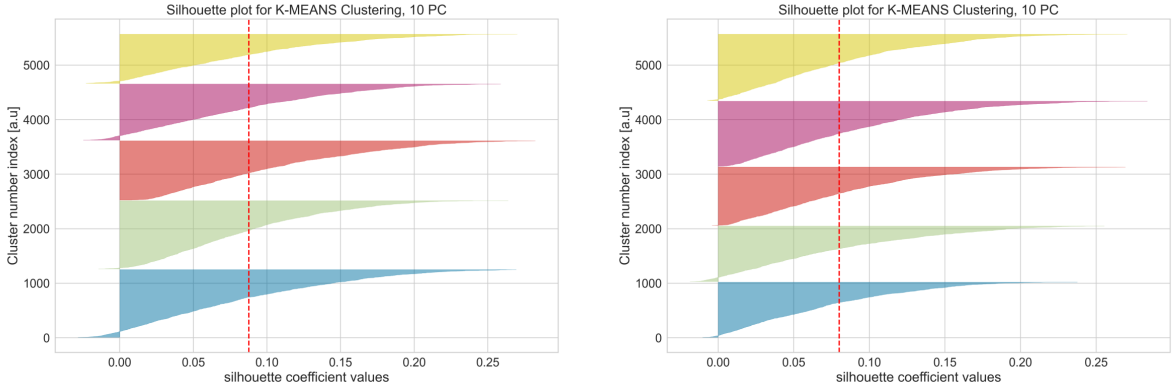

(a) North Atlantic-Eurasian region

(b) Arctic region

Figure B2. The following figure depicts the silhouette plot for both regions under consideration. The cluster number index represents the number of days assigned to the centroids in the KME algorithm within the specified time periods, which total 5520 days. In the calculations, leap days are not included. The principal components (PC) are indicated during the calculation of the centroids in the KME algorithm.

https://doi.org/10.5194/egusphere-2025-1373
Preprint. Discussion started: 9 April 2025

Appendix C: Sensitivity Tests on Arctic Region

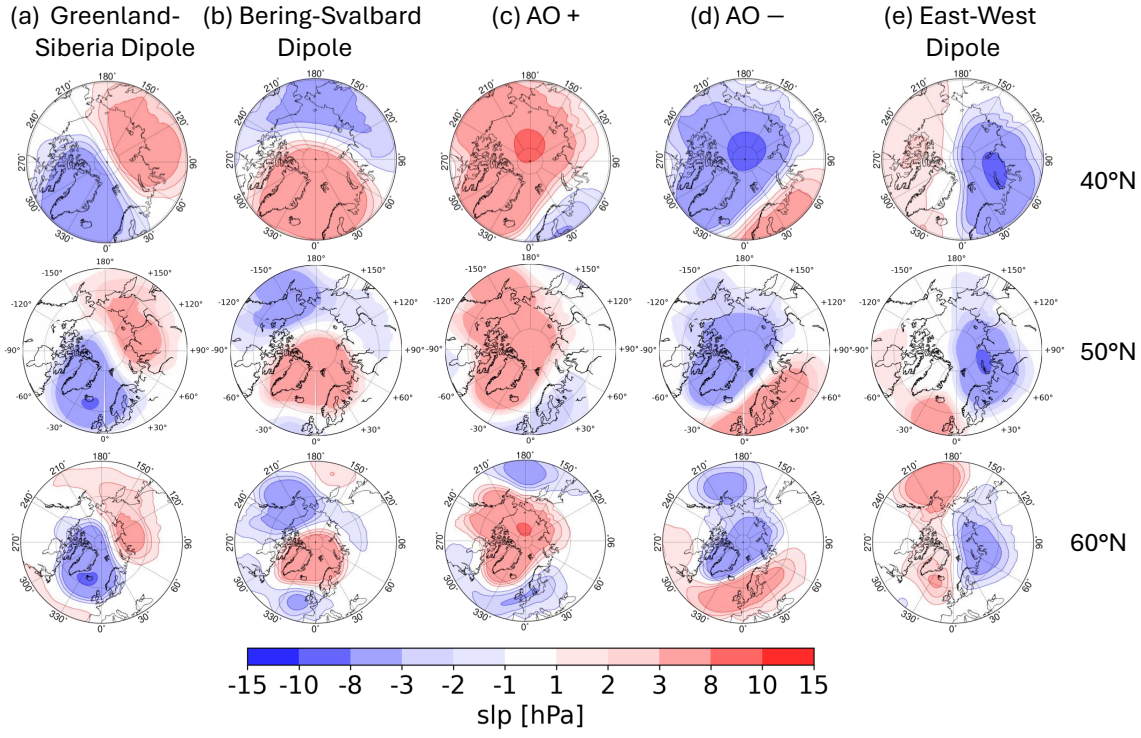

Figure C1. Reference circulation regimes ERA5 for the Arctic region in the historical time period 1985-2014 for different constraints calculated by the KME algorithm in the extended boreal summer season from May to October

In contrast to the North Atlantic-Eurasian region, where Dorrington and Strommen (2020); Boé et al. (2009); Crasemann et al. (2017); Riebold (2023) have observed comparable regions, there is currently no consensus on the dimensions and confinement of the Arctic region to investigate within the circumpolar Arctic during the summer season (Proshutinsky et al., 2015; Wang et al., 2021; Timmermans and Marshall, 2020). If the region is defined too narrowly, for example, as 60°N to 90°N, the resulting clusters are geometrically constrained, refer Fig. C1, bottom row. The storm track route is located approximately at 60°, leading to patterns that are more geometrical than physically reasonable if the investigated area is confined to 60°N. The aforementioned constraints are not observed when the region is extended to 50°N or 40°N, where the calculated patterns from the K-Means algorithm exhibit a similar spatial structure refer to Fig. C1, center and top row. Therefore, the region under consideration is defined as the smallest area that still exhibits physical patterns in the Arctic region, spanning 50°N to 90°N and covering the entire circumpolar region.

https://doi.org/10.5194/egusphere-2025-1373
Preprint. Discussion started: 9 April 2025

Author contributions. DH and OL developed the original idea for the paper. JM conducted the data analysis for KME and the visualisations except Figure 10 and wrote most of the paper. OL performed the analysis for SAN algorithm. DH and OL commented on, organised and wrote parts of the paper.

Competing interests. The authors declare that they have no conflict of interest.

Acknowledgements. We acknowledge Xavier Levine for providing the panels used in Figure 10.This work was conducted as part of the EU Horizon 2020 POLARRES project (grant number 101003590). OAL was also supported with computational resources from the National Infrastructure for High Performance Computing and Data Storage in Norway (Sigma2), projects NN8002K and NN9870K. DH gratefully acknowledges the support from the Transregional Collaborative Research Center (TR 172) "ArctiC Amplification: Climate Relevant Atmospheric and SurfaCe Processes, and Feedback Mechanisms (AC)3" (project ID 268020496), which is funded by the German Research Foundation (DFG, Deutsche Forschungsgemeinschaft) and the support from the German Federal Ministry for Education and Re- search (BMBF) project "TurbO-Arctic" (01LK2317A) of the "WarmWorld Smarter" program. JM and DH were also supported by the Deutsches Klimarechenzentrum (DKRZ) in Hamburg which provided computational resources and the technical infrastructure for the analysis.

https://doi.org/10.5194/egusphere-2025-1373
Preprint. Discussion started: 9 April 2025

References

Babanov, B. A., Semenov, V. A., Akperov, M. G., Mokhov, I. I., and Keenlyside, N. S.: Occurrence of Winter Atmospheric Circulation Regimes in Euro-Atlantic Region and Associated Extreme Weather Anomalies in the Northern Hemisphere, Atmospheric and Oceanic Optics, 36, 522–531, https://doi.org/10.1134/S1024856023050056, 2023.

Barnes, E. A. and Polvani, L.: Response of the Midlatitude Jets, and of Their Variability, to Increased Greenhouse Gases in the CMIP5 Models, Journal of Climate, 26, 7117 – 7135, https://doi.org/10.1175/JCLI-D-12-00536.1, 2013.

Benestad, R. E., Mezghani, A., Lutz, J., Dobler, A., Parding, K. M., and Landgren, O. A.: Various ways of using empirical orthogonal functions for climate model evaluation, Geoscientific Model Development, 16, 2899–2913, https://doi.org/10.5194/gmd-16-2899-2023, 2023.

Bi, D., Dix, M., Marsland, S., O'Farrell, S., Sullivan, A., Bodman, R., Law, R., Harman, I., Srbinovsky, J., Rashid, H. A., Dobrohotoff, P., Mackallah, C., Yan, H., Hirst, A., Savita, A., Dias, F. B., Woodhouse, M., Fiedler, R., and Heerdegen, A.: Configuration and spin-up of ACCESS-CM2, the new generation Australian Community Climate and Earth System Simulator Coupled Model, Journal of Southern Hemisphere Earth Systems Science, 70, 225–251, https://doi.org/10.1071/ES19040, 2020.

Boucher, O., Servonnat, J., Albright, A. L., Aumont, O., Balkanski, Y., Bastrikov, V., Bekki, S., Bonnet, R., Bony, S., Bopp, L., Braconnot, P., Brockmann, P., Cadule, P., Caubel, A., Cheruy, F., Codron, F., Cozic, A., Cugnet, D., D'Andrea, F., Davini, P., de Lavergne, C., Denvil, S., Deshayes, J., Devilliers, M., Ducharne, A., Dufresne, J.-L., Dupont, E., Éthé, C., Fairhead, L., Falletti, L., Flavoni, S., Foujols, M.-A., Gardoll, S., Gastineau, G., Ghattas, J., Grandpeix, J.-Y., Guenet, B., Guez, Lionel, E., Guilyardi, E., Guimberteau, M., Hauglustaine, D., Hourdin, F., Idelkadi, A., Joussaume, S., Kageyama, M., Khodri, M., Krinner, G., Lebas, N., Levavasseur, G., Lévy, C., Li, L., Lott, F., Lurton, T., Luyssaert, S., Madec, G., Madeleine, J.-B., Maignan, F., Marchand, M., Marti, O., Mellul, L., Meurdesoif, Y., Mignot, J., Musat, I., Ottlé, C., Peylin, P., Planton, Y., Polcher, J., Rio, C., Rochetin, N., Rousset, C., Sepulchre, P., Sima, A., Swingedouw, D., Thiéblemont, R., Traore, A. K., Vancoppenolle, M., Vial, J., Vialard, J., Viovy, N., and Vuichard, N.: Presentation and Evaluation of the IPSL-CM6A-LR Climate Model, Journal of Advances in Modeling Earth Systems, 12, e2019MS002 010, https://doi.org/https://doi.org/10.1029/2019MS002010, e2019MS002010 10.1029/2019MS002010, 2020.

Boé, J., Terray, L., Cassou, C., and Najac, J.: Uncertainties in European summer precipitation changes: Role of large scale circulation, Climate Dynamics, 33, 265–276, https://doi.org/10.1007/s00382-008-0474-7, 2009.

Brunner, L., Schaller, N., Anstey, J., Sillmann, J., and Steiner, A. K.: Dependence of Present and Future European Temperature Extremes on the Location of Atmospheric Blocking, Geophysical Research Letters, 45, 6311–6320, https://doi.org/https://doi.org/10.1029/2018GL077837, 2018.

Byun, Y.-H., Lim, Y.-J., Sung, H. M., Kim, J., Sun, M., and Kim, B.-H.: NIMS-KMA KACE1.0-G model output prepared for CMIP6 CMIP, https://doi.org/10.22033/ESGF/CMIP6.2241, 2019.

Cattiaux, J., Vautard, R., Cassou, C., Yiou, P., Masson-Delmotte, V., and Codron, F.: Winter 2010 in Europe: A cold extreme in a warming climate, Geophysical Research Letters, 37, https://doi.org/https://doi.org/10.1029/2010GL044613, 2010.

Cattiaux, J., Douville, H., and Peings, Y.: European temperatures in CMIP5: origins of present-day biases and future uncertainties, Climate Dynamics, 41, 2889–2907, https://doi.org/10.1007/s00382-013-1731-y, 2013.

Corti, S., Molteni, F., and Palmer, T. N.: Signature of recent climate change in frequencies of natural atmospheric circulation regimes, Nature, 398, 799–802, https://doi.org/10.1038/19745, 1999.

https://doi.org/10.5194/egusphere-2025-1373
Preprint. Discussion started: 9 April 2025

Coumou, D. and Rahmstorf, S.: A decade of weather extremes, Nature Climate Change, 2, 491–496, https://doi.org/10.1038/nclimate1452, 2012.

Crasemann, B., Handorf, D., Jaiser, R., Dethloff, K., Nakamura, T., Ukita, J., and Yamazaki, K.: Can preferred atmospheric circulation patterns over the North-Atlantic-Eurasian region be associated with arctic sea ice loss?, Polar Science, 14, 9–20, https://doi.org/https://doi.org/10.1016/j.polar.2017.09.002, 2017.

Danabasoglu, G., Lamarque, J.-F., Bacmeister, J., Bailey, D. A., DuVivier, A. K., Edwards, J., Emmons, L. K., Fasullo, J., Garcia, R., Gettelman, A., Hannay, C., Holland, M. M., Large, W. G., Lauritzen, P. H., Lawrence, D. M., Lenaerts, J. T. M., Lindsay, K., Lipscomb, W. H., Mills, M. J., Neale, R., Oleson, K. W., Otto-Bliesner, B., Phillips, A. S., Sacks, W., Tilmes, S., van Kampenhout, L., Vertenstein, M., Bertini, A., Dennis, J., Deser, C., Fischer, C., Fox-Kemper, B., Kay, J. E., Kinnison, D., Kushner, P. J., Larson, V. E., Long, M. C., Mickelson, S., Moore, J. K., Nienhouse, E., Polvani, L., Rasch, P. J., and Strand, W. G.: The Community Earth System Model Version 2 (CESM2), Journal of Advances in Modeling Earth Systems, 12, e2019MS001 916, https://doi.org/https://doi.org/10.1029/2019MS001916, e2019MS001916 2019MS001916, 2020.

Dorrington, J. and Strommen, K. J.: Jet Speed Variability Obscures Euro-Atlantic Regime Structure, Geophysical Research Letters, 47, e2020GL087 907, https://doi.org/https://doi.org/10.1029/2020GL087907, e2020GL087907 10.1029/2020GL087907, 2020.

Dorrington, J., Strommen, K., and Fabiano, F.: Quantifying climate model representation of the wintertime Euro-Atlantic circulation using geopotential-jet regimes, Weather and Climate Dynamics, 3, 505–533, https://doi.org/10.5194/wcd-3-505-2022, 2022.

Dunne, J., Horowitz, L., Adcroft, A., Ginoux, P., Held, I., John, J., Krasting, J., Malyshev, S., Naik, V., Paulot, F., Shevliakova, E., Stock, C., Zadeh, N., Balaji, V., Blanton, C., Dunne, K., Dupuis, C., Durachta, J., Dussin, R., and Zhao, M.: The GFDL Earth System Model version 4.1 (GFDL-ESM 4.1): Overall coupled model description and simulation characteristics, Journal of Advances in Modeling Earth Systems, 12, e2019MS002 015, https://doi.org/10.1029/2019MS002015, 2020.

Fabiano, F., Meccia, V. L., Davini, P., Ghinassi, P., and Corti, S.: A regime view of future atmospheric circulation changes in northern mid-latitudes, Weather and Climate Dynamics, 2, 163–180, https://doi.org/10.5194/wcd-2-163-2021, 2021.

Hajima, T., Watanabe, M., Yamamoto, A., Tatebe, H., Noguchi, M. A., Abe, M., Ohgaito, R., Ito, A., Yamazaki, D., Okajima, H., Ito, A., Takata, K., Ogochi, K., Watanabe, S., and Kawamiya, M.: Development of the MIROC-ES2L Earth system model and the evaluation of biogeochemical processes and feedbacks, Geoscientific Model Development, 13, 2197–2244, https://doi.org/10.5194/gmd-13-2197-2020, 2020.

Hannachi, A., Straus, D. M., Franzke, C. L., Corti, S., and Woollings, T.: Low-frequency nonlinearity and regime behavior in the Northern Hemisphere extratropical atmosphere, Reviews of Geophysics, 55, 199–234, https://agupubs.onlinelibrary.wiley.com/doi/full/10.1002/2015RG000509, 2017.

Held, I. M., Guo, H., Adcroft, A., Dunne, J. P., Horowitz, L. W., Krasting, J., Shevliakova, E., Winton, M., Zhao, M., Bushuk, M., Wittenberg, A. T., Wyman, B., Xiang, B., Zhang, R., Anderson, W., Balaji, V., Donner, L., Dunne, K., Durachta, J., Gauthier, P. P. G., Ginoux, P., Golaz, J.-C., Griffies, S. M., Hallberg, R., Harris, L., Harrison, M., Hurlin, W., John, J., Lin, P., Lin, S.-J., Malyshev, S., Menzel, R., Milly, P. C. D., Ming, Y., Naik, V., Paynter, D., Paulot, F., Ramaswamy, V., Reichl, B., Robinson, T., Rosati, A., Seman, C., Silvers, L. G., Underwood, S., and Zadeh, N.: Structure and Performance of GFDL's CM4.0 Climate Model, Journal of Advances in Modeling Earth Systems, 11, 3691–3727, https://doi.org/https://doi.org/10.1029/2019MS001829, 2019.

Hersbach, H., Bell, B., Berrisford, P., Hirahara, S., Horányi, A., Muñoz-Sabater, J., Nicolas, J., Peubey, C., Radu, R., Schepers, D., Simmons, A., Soci, C., Abdalla, S., Abellan, X., Balsamo, G., Bechtold, P., Biavati, G., Bidlot, J., Bonavita, M., De Chiara, G., Dahlgren, P., Dee, D., Diamantakis, M., Dragani, R., Flemming, J., Forbes, R., Fuentes, M., Geer, A., Haimberger, L., Healy, S., Hogan, R. J.,

https://doi.org/10.5194/egusphere-2025-1373
Preprint. Discussion started: 9 April 2025

Hólm, E., Janisková, M., Keeley, S., Laloyaux, P., Lopez, P., Lupu, C., Radnoti, G., de Rosnay, P., Rozum, I., Vamborg, F., Villaume, S., and Thépaut, J.-N.: The ERA5 global reanalysis, Quarterly Journal of the Royal Meteorological Society, 146, 1999–2049, https://doi.org/https://doi.org/10.1002/qj.3803, 2020.

Horton, R. M., Coffel, E. D., Winter, J. M., and Bader, D. A.: Projected changes in extreme temperature events based on the NARCCAP model suite, Geophysical Research Letters, 42, 7722–7731, https://doi.org/10.1002/2015GL064914, 2015.

Hoskins, B. and Woollings, T.: Persistent Extratropical Regimes and Climate Extremes, Current Climate Change Reports, 1, 115–124, https://doi.org/10.1007/s40641-015-0020-8, 2015.

Levine, X. J., Williams, R. S., Marshall, G., Orr, A., Seland Graff, L., Handorf, D., Karpechko, A., Köhler, R., Wijngaard, R. R., Johnston, N., Lee, H., Nieradzik, L., and Mooney, P. A.: Storylines of summer Arctic climate change constrained by Barents–Kara seas and Arctic tropospheric warming for climate risk assessment, Earth System Dynamics, 15, 1161–1177, https://doi.org/10.5194/esd-15-1161-2024, 2024.

Lorenz, E.: Empirical Orthogonal Functions and Statistical Weather Prediction, Science Report 1, Massachusetts Institute of Technology, https://doi.org/http://www.o3d.org/abracco/Atlantic/Lorenz1956.pdf, 1956.

Madonna, E., Li, C., Grams, C. M., and Woollings, T.: The link between eddy-driven jet variability and weather regimes in the North Atlantic-European sector, Quarterly Journal of the Royal Meteorological Society, 143, 2960–2972, https://doi.org/https://doi.org/10.1002/qj.3155, 2017.

Mauritsen, T., Bader, J., Becker, T., Behrens, J., Bittner, M., Brokopf, R., Brovkin, V., Claussen, M., Crueger, T., Esch, M., Fast, I., Fiedler, S., Fläschner, D., Gayler, V., Giorgetta, M., Goll, D., Haak, H., Hagemann, S., Hedemann, C., and Roeckner, E.: Developments in the MPI-M Earth System Model version 1.2 (MPI-ESM 1.2) and its response to increasing CO 2, Journal of Advances in Modeling Earth Systems, 11, https://doi.org/10.1029/2018MS001400, 2019.

Olmo, M., Cos, P., Ángel G. Muñoz, Altava-Ortiz, V., Barrera-Escoda, A., Campos, D., Soret, A., and Doblas-Reyes, F.: Cross-Time-Scale Analysis of Year-Round Atmospheric Circulation Patterns and Their Impacts on Rainfall and Temperatures in the Iberian Peninsula, Journal of Climate, 37, 5525 – 5541, https://doi.org/10.1175/JCLI-D-23-0735.1, 2024.

Palmer, T. N.: A nonlinear dynamical perspective on climate change, Weather, 48, 314–326, https://doi.org/https://doi.org/10.1002/j.1477-8696.1993.tb05802.x, 1993.

Philipp, A., Della-Marta, P. M., Jacobeit, J., Fereday, D. R., Jones, P. D., Moberg, A., and Wanner, H.: Long-Term Variability of Daily North Atlantic–European Pressure Patterns since 1850 Classified by Simulated Annealing Clustering, Journal of Climate, 20, 4065 – 4095, https://doi.org/10.1175/JCLI4175.1, 2007.

Philipp, A., Beck, C., Huth, R., and Jacobeit, J.: Development and comparison of circulation type classifications using the COST 733 dataset and software, https://opus.bibliothek.uni-augsburg.de/opus4/files/40073/40073.pdf, 2016.

Proshutinsky, A., Dukhovskoy, D., Timmermans, M.-L., Krishfield, R., and Bamber, J. L.: Arctic circulation regimes, Philosophical Transactions of the Royal Society A: Mathematical, Physical and Engineering Sciences, 373, 20140 160, https://doi.org/10.1098/rsta.2014.0160, 2015.

Riebold, J.: On the linkage between future Arctic sea ice retreat, the large-scale atmospheric circulation and temperature extremes over Europe, doctoralthesis, Universität Potsdam, https://doi.org/10.25932/publishup-60488, 2023.

Røste, J. and Landgren, O. A.: Impacts of dynamical downscaling on circulation type statistics in the Euro-CORDEX ensemble, Climate Dynamics, 59, 2445–2466, https://doi.org/https://doi.org/10.1007/s00382-022-06219-y, 2022.

https://doi.org/10.5194/egusphere-2025-1373
Preprint. Discussion started: 9 April 2025

Rousseeuw, P. J.: Silhouettes: A graphical aid to the interpretation and validation of cluster analysis, Journal of Computational and Applied Mathematics, 20, 53–65, https://doi.org/https://doi.org/10.1016/0377-0427(87)90125-7, 1987.

Scaife, A. A. and Smith, D.: A signal-to-noise paradox in climate science, npj Climate and Atmospheric Science, 1, 28, https://doi.org/10.1038/s41612-018-0038-4, 2018.

Schaller, N., Sillmann, J., Anstey, J., Fischer, E. M., Grams, C. M., and Russo, S.: Influence of blocking on Northern European and Western Russian heatwaves in large climate model ensembles, Environmental Research Letters, 13, 054 015, https://doi.org/10.1088/1748-9326/aaba55, 2018.

Screen, J. A. and Simmonds, I.: The central role of diminishing sea ice in recent Arctic temperature amplification, Nature, 464, 1334–1337, https://doi.org/10.1038/nature09051, 2010.

Seferian, R.: CNRM-CERFACS CNRM-ESM2-1 model output prepared for CMIP6 CMIP, https://doi.org/10.22033/ESGF/CMIP6.1391, 2018.

Seland, Ø., Bentsen, M., Olivié, D., Toniazzo, T., Gjermundsen, A., Graff, L. S., Debernard, J. B., Gupta, A. K., He, Y.-C., Kirkevåg, A., Schwinger, J., Tjiputra, J., Aas, K. S., Bethke, I., Fan, Y., Griesfeller, J., Grini, A., Guo, C., Ilicak, M., Karset, I. H. H., Landgren, O., Liakka, J., Moseid, K. O., Nummelin, A., Spensberger, C., Tang, H., Zhang, Z., Heinze, C., Iversen, T., and Schulz, M.: Overview of the Norwegian Earth System Model (NorESM2) and key climate response of CMIP6 DECK, historical, and scenario simulations, Geoscientific Model Development, 13, 6165–6200, https://doi.org/10.5194/gmd-13-6165-2020, 2020.

Sellar, A. A., Jones, C. G., Mulcahy, J. P., Tang, Y., Yool, A., Wiltshire, A., O'Connor, F. M., Stringer, M., Hill, R., Palmieri, J., Woodward, S., de Mora, L., Kuhlbrodt, T., Rumbold, S. T., Kelley, D. I., Ellis, R., Johnson, C. E., Walton, J., Abraham, N. L., Andrews, M. B., Andrews, T., Archibald, A. T., Berthou, S., Burke, E., Blockley, E., Carslaw, K., Dalvi, M., Edwards, J., Folberth, G. A., Gedney, N., Griffiths, P. T., Harper, A. B., Hendry, M. A., Hewitt, A. J., Johnson, B., Jones, A., Jones, C. D., Keeble, J., Liddicoat, S., Morgenstern, O., Parker, R. J., Predoi, V., Robertson, E., Siahaan, A., Smith, R. S., Swaminathan, R., Woodhouse, M. T., Zeng, G., and Zerroukat, M.: UKESM1: Description and Evaluation of the U.K. Earth System Model, Journal of Advances in Modeling Earth Systems, 11, 4513–4558, https://doi.org/https://doi.org/10.1029/2019MS001739, 2019.

Seneviratne, S. I., Zhang, X., Adnan, M., Badi, W., Dereczynski, C., Luca, A. D., Ghosh, S., Iskandar, I., Kossin, J., Lewis, S., Otto, F., Pinto, I., Satoh, M., Vicente-Serrano, S. M., Wehner, M., Zhou, B., and Allan, R.: Weather and Climate Extreme Events in a Changing Climate, p. 1513–1766, Cambridge University Press, https://doi.org/10.1017/9781009157896.013, 2021.

Shepherd, T. G.: A Common Framework for Approaches to Extreme Event Attribution, Current Climate Change Reports, 2, 28–38, https://doi.org/10.1007/s40641-016-0033-y, 2016.

Shepherd, T. G., Boyd, E., Calel, R. A., Chapman, S. C., Dessai, S., Dima-West, I. M., Fowler, H. J., James, R., Maraun, D., Martius, O., Senior, C. A., Sobel, A. H., Stainforth, D. A., Tett, S. F. B., Trenberth, K. E., van den Hurk, B. J. J. M., Watkins, N. W., Wilby, R. L., and Zenghelis, D. A.: Storylines: an alternative approach to representing uncertainty in physical aspects of climate change, Climatic Change, 151, 555–571, https://doi.org/10.1007/s10584-018-2317-9, 2018.

Smith, D. M., Gillett, N. P., Simpson, I. R., Athanasiadis, P. J., Baehr, J., Bethke, I., Bilge, T. A., Bonnet, R., Boucher, O., Findell, K. L., Gastineau, G., Gualdi, S., Hermanson, L., Leung, L. R., Mignot, J., Müller, W. A., Osprey, S., Otterå, O. H., Persad, G. G., Scaife, A. A., Schmidt, G. A., Shiogama, H., Sutton, R. T., Swingedouw, D., Yang, S., Zhou, T., and Ziehn, T.: Attribution of multi-annual to decadal changes in the climate system: The Large Ensemble Single Forcing Model Intercomparison Project (LESFMIP), Frontiers in Climate, 4, 955 414, https://doi.org/10.3389/fclim.2022.955414, 2022.

https://doi.org/10.5194/egusphere-2025-1373
Preprint. Discussion started: 9 April 2025

Sousa, P. M., Trigo, R. M., Barriopedro, D., Soares, P. M. M., and Santos, J. A.: European temperature responses to blocking and ridge regional patterns, Climate Dynamics, 50, 457–477, https://doi.org/10.1007/s00382-017-3620-2, 2018.

Stephenson, D. B., Hannachi, A., and O'Neill, A.: On the existence of multiple climate regimes, Quarterly Journal of the Royal Meteorological Society, 130, 583–605, https://doi.org/https://doi.org/10.1256/qj.02.146, 2004.

Straus, D. M., Corti, S., and Molteni, F.: Circulation Regimes: Chaotic Variability versus SST-Forced Predictability, Journal of Climate, 20, 2251 – 2272, https://doi.org/https://doi.org/10.1175/JCLI4070.1, 2007.

Tatebe, H., Ogura, T., Nitta, T., Komuro, Y., Ogochi, K., Takemura, T., Sudo, K., Sekiguchi, M., Abe, M., Saito, F., Chikira, M., Watanabe, S., Mori, M., Hirota, N., Kawatani, Y., Mochizuki, T., Yoshimura, K., Takata, K., O'ishi, R., Yamazaki, D., Suzuki, T., Kurogi, M., Kataoka, T., Watanabe, M., and Kimoto, M.: Description and basic evaluation of simulated mean state, internal variability, and climate sensitivity in MIROC6, Geoscientific Model Development, 12, 2727–2765, https://doi.org/10.5194/gmd-12-2727-2019, 2019.

Taylor, K. E.: Summarizing multiple aspects of model performance in a single diagram, Journal of Geophysical Research: Atmospheres, 106, 7183–7192, https://doi.org/https://doi.org/10.1029/2000JD900719, 2001.

Timmermans, M.-L. and Marshall, J.: Understanding Arctic Ocean Circulation: A Review of Ocean Dynamics in a Changing Climate, Journal of Geophysical Research: Oceans, 125, e2018JC014 378, https://doi.org/https://doi.org/10.1029/2018JC014378, e2018JC014378 10.1029/2018JC014378, 2020.

Trenberth, K. E., Fasullo, J. T., and Shepherd, T. G.: Attribution of climate extreme events, Nature Climate Change, 5, 725–730, https://doi.org/10.1038/nclimate2657, 2015.

Tveito, O. E. and Huth, R.: Circulation-type classifications in Europe: results of the COST 733 Action, International Journal of Climatology, 7, 2671–2672, 2016.

Voldoire, A., Saint-Martin, D., Sénési, S., Decharme, B., Alias, A., Chevallier, M., Colin, J., Guérémy, J.-F., Michou, M., Moine, M.-P., Nabat, P., Roehrig, R., Salas y Mélia, D., Séférian, R., Valcke, S., Beau, I., Belamari, S., Berthet, S., Cassou, C., Cattiaux, J., Deshayes, J., Douville, H., Ethé, C., Franchistéguy, L., Geoffroy, O., Lévy, C., Madec, G., Meurdesoif, Y., Msadek, R., Ribes, A., Sanchez-Gomez, E., Terray, L., and Waldman, R.: Evaluation of CMIP6 DECK Experiments With CNRM-CM6-1, Journal of Advances in Modeling Earth Systems, 11, 2177–2213, https://doi.org/https://doi.org/10.1029/2019MS001683, 2019.

Volodin, E., Mortikov, E., Gritsun, A., Lykossov, V., Galin, V., Diansky, N., Gusev, A., Kostrykin, S., Iakovlev, N., Shestakova, A., and Emelina, S.: INM INM-CM4-8 model output prepared for CMIP6 ScenarioMIP, https://doi.org/10.22033/ESGF/CMIP6.12321, 2019.

Wang, Q., Danilov, S., Sidorenko, D., and Wang, X.: Circulation Pathways and Exports of Arctic River Runoff Influenced by Atmospheric Circulation Regimes, Frontiers in Marine Science, 8, https://doi.org/10.3389/fmars.2021.707593, 2021.

Welch, B.: THE GENERALIZATION OF 'STUDENT'S' PROBLEM WHEN SEVERAL DIFFERENT POPULATION VARLANCES ARE INVOLVED, Biometrika, 34, 28–35, https://doi.org/10.1093/biomet/34.1-2.28, 1947.

Wiel, K., Bloomfield, H., Lee, R., Stoop, L., Blackport, R., Screen, J., and Selten, F.: The influence of weather regimes on European renewable energy production and demand, Environmental Research Letters, https://doi.org/10.1088/1748-9326/ab38d3, 2019.

Williams, K. D., Copsey, D., Blockley, E. W., Bodas-Salcedo, A., Calvert, D., Comer, R., Davis, P., Graham, T., Hewitt, H. T., Hill, R., Hyder, P., Ineson, S., Johns, T. C., Keen, A. B., Lee, R. W., Megann, A., Milton, S. F., Rae, J. G. L., Roberts, M. J., Scaife, A. A., Schiemann, R., Storkey, D., Thorpe, L., Watterson, I. G., Walters, D. N., West, A., Wood, R. A., Woollings, T., and Xavier, P. K.: The Met Office Global Coupled Model 3.0 and 3.1 (GC3.0 and GC3.1) Configurations, Journal of Advances in Modeling Earth Systems, 10, 357–380, https://doi.org/https://doi.org/10.1002/2017MS001115, 2018.

https://doi.org/10.5194/egusphere-2025-1373
Preprint. Discussion started: 9 April 2025

Woollings, T. and Blackburn, M.: The North Atlantic Jet Stream under Climate Change and Its Relation to the NAO and EA Patterns, Journal of Climate, 25, 886 – 902, https://doi.org/10.1175/JCLI-D-11-00087.1, 2012.

Yukimoto, S., KAWAI, H., KOSHIRO, T., OSHIMA, N., YOSHIDA, K., URAKAWA, S., TSUJINO, H., DEUSHI, M., TANAKA, T., HOSAKA, M., YABU, S., YOSHIMURA, H., SHINDO, E., MIZUTA, R., OBATA, A., ADACHI, Y., and ISHII, M.: The Meteorological Research Institute Earth System Model Version 2.0, MRI-ESM2.0: Description and Basic Evaluation of the Physical Component, Journal of the Meteorological Society of Japan. Ser. II, 97, 931–965, https://doi.org/10.2151/jmsj.2019-051, 2019.

Ziehn, T., Chamberlain, M. A., Law, R. M., Lenton, A., Bodman, R. W., Dix, M., Stevens, L., Wang, Y.-P., and Srbinovsky, J.: The Australian Earth System Model: ACCESS-ESM1.5, Journal of Southern Hemisphere Earth Systems Science, 70, 193–214, https://doi.org/10.1071/ES19035, 2020.